# BUCKLING OF BEAMS AND COATINGS OF FINITE WIDTH IN BILATERAL FRICTIONLESS CONTACT WITH AN ELASTIC HALF-SPACE

Daniele BARALDI[a], Nerio TULLINI[b]

[a] corresponding author; Università IUAV di Venezia, Italy; e-mail: danielebaraldi@iuav.it

[b] Department of Engineering; University of Ferrara, Italy; e-mail: nerio.tullini@unife.it

## ABSTRACT

In this work, a simple and efficient finite element-boundary integral equation coupling method is adopted for studying the buckling of beams and coatings resting on a three-dimensional elastic half-space. For this purpose, a mixed variational formulation based on the Green function of the substrate is adopted by assuming as independent fields beam displacements and contact pressures. Euler-Bernoulli beams with finite width and different combinations of end restraints are considered. Some numerical tests illustrate the accuracy of the proposed formulation, with particular attention to the convergence to existing analytical and numerical solutions and to the proposal of new estimates of beams and coatings buckling wavelength and critical loads for varying length-to-width ratio and beam-substrate relative stiffness.

## KEYWORDS

Beam; Coatings; Buckling; Transversely isotropic elastic half-space; Boussinesq solution; Frictionless bilateral contact; Mixed variational principle.

## 1. INTRODUCTION

The buckling of beams resting on an elastic substrate, soil, or foundation is a research topic that involves many engineering fields and it was studied in the past by many researchers. In the civil engineering field, examples of this problem are the buckling of highway or aircraft concrete pavements. In this context, the pioneering works of Wieghardt (1922) and Prager (1927) are based on the assumption that the beam is resting on a continuously distributed set of springs (Winkler, 1867),. However, the actual response at the interface between the beam and the substrate is very difficult to be determined; hence, many foundation models can be found in literature for approximating the actual foundation behaviour (Selvadurai, 1979a). The first analytical approach for solving the problem of a beam on a semi-infinite elastic medium was performed by Biot (1937), who studied the bending of an infinite beam resting either on a two- or three-dimensional elastic half-space. In the same year, Reissner (1937) studied the stability problem of an infinite beam resting on a two-dimensional elastic support, whereas some decades later Murthy (1973) adopted Biot results for comparing the buckling of continuously supported beams on two- and three-dimensional half-space, showing the effect of a foundation extending beyond the width of the beam.

After the first pioneering works, the problem of a beam on elastic substrate, with particular attention to its stability, grew motivated by early structural problems of sandwich panels in airplanes (Allen, 1969). In particular, Gough et al. (1940) extended Biot and Reissner results of a beam on two-dimensional elastic half-space by considering various conditions of contact between the infinite beam and the half-plane. Further research activities on sandwich elements continued up to recent years (Ley et a., 1999; Davies, 2001) and also the buckling of concrete pavements and welded rails was studied (Kerr, 1974; Kerr, 1978; Kerr, 1984; Lim et al., 2003).

Recently, the stability of a beam on elastic half-space has been taken into consideration for the analytical and numerical simulation of the buckling of thin films on compliant substrates, and the research has been driven by developments in electronic industry (Shield et al. 1994; Bowden et al., 1999; Volynskii et al., 2000), with particular reference to stretchable electronic interconnects and devices (see Jiang et al. (2008) and references cited therein). The case of buckling without delamination is often called wrinkling (Genzer and Groenewold, 2006). In this field, the adoption of a beam model, in particular an Euler-Bernoulli one, on a semi-infinite elastic half-space is justified by the thickness of the support, which is often four order of magnitude larger than the film thickness. Furthermore, the contact is assumed to be frictionless, since it was demonstrated that the shear stresses at the interface between the film and the compliant substrate has a negligible effect on the buckling of the system (Huang, 2005).

Considering microelectronic devices, the mechanical properties of thin films can be estimated by observing buckling patterns (Stafford et al., 2004; Wilder et al., 2006), and the buckling wavelength and amplitude are important for stretchable and flexible electronics. Many mechanical models have been developed in recent years (Huang and Suo, 2002a; Huang and Suo, 2002b; Stafford et al., 2004; Huang, 2005; Wilder et al., 2006) for understanding the relationship between buckling profiles and material parameters. Recent advances on buckling of thin films on a bi-layer compliant substrate of finite thickness can be found in Wang et al. (2020) and references cited therein. However, most of the existing mechanical models assume plane-strain deformation hypothesis, which is not always adequate, especially in case of narrow thin films on compliant substrates, as it has been recently pointed out by Jiang et al. (2008) by determining an analytical solution for the buckling of an Euler-Bernoulli beam on three-dimensional half-space and comparing analytical results with experimental data.

It is worth noting that most of the contributions dedicated to buckling of beams on elastic substrates, both regarding civil or mechanical/electronic engineering, assume the hypothesis of beams with infinite length; however, in some cases, with particular reference to shallow foundations in civil engineering, the beam length is finite and at least one order of magnitude larger than beam width; furthermore, the structural relationship between the foundation beam and the superstructure may need to be taken into consideration by adopting appropriate boundary conditions at beam ends.

Focusing on the buckling of beams with finite length, in Timoshenko and Gere (1961) a simply supported beam on Winkler soil was studied. Other boundary conditions, such as beam with fixed ends and beam with free ends, were studied and compared with the former (Hetenyi, 1946). In the context of sandwich plates, even if still modelled as beams on Winkler support, the finite length of the beam allowed Goodier and Hsu (1954) to highlight the presence of nonsinusoidal buckling modes with displacements localized at the beam ends. Similar local buckling modes have been recently found by Tullini et al. (2013a) with a beam having free and pinned ends on a two-dimensional elastic medium; furthermore, the corresponding critical loads led to critical stresses lower than that typically assumed for sandwich panel design and derived from Reissner solution.

In the present work, the buckling of Euler-Bernoulli beams with finite length resting in bilateral frictionless contact with an elastic three-dimensional half-space is studied by extending to this field of analysis the finite element-boundary integral equation (FE-BIE) coupling method introduced in Tullini and Tralli (2010) for the static analysis of foundation beams with varying boundary conditions. This method has already proven its effectiveness by comparing numerical results of static analyses with exiting analytical solutions and other numerical results. In particular, the computational effort required by proposed method turned out to be significantly smaller than that of a standard Finite Element Model (FEM).

The FE-BIE coupling method has been originally introduced for the static analysis of both Euler-Bernoulli and Timoshenko beams in frictionless contact with a two-dimensional half-space (Tullini and Tralli, 2010) and it has been already extended to the corresponding buckling problem (Tullini et al., 2013a, Tullini et al., 2013b, Baraldi, 2019), and to the case of a fully adhesive contact (Tullini et al., 2012; Tezzon et al. 2015; Tezzon et al. 2016; Tezzon et al. 2018). Effects of sharp and smooth beam edges in the buckling of a Timoshenko beam in frictionless and bilateral contact with an elastic half-plane was analysed in Falope et al. (2020).

Here, attention is given to Euler-Bernoulli beams resting on a three-dimensional transversely isotropic elastic half-space, having the plane of isotropy parallel to the half-space boundary. The beam instability in horizontal direction, which may take place with beams having large length-to-width ratio (Kerr, 1974; Kerr, 1978), here is neglected and only vertical displacements are taken into account. Beam deflections are assumed to vary only along longitudinal direction, hence uniform displacements along beam transversal direction are assumed. The proposed mixed variational formulation assumes as independent fields both the surface tractions and the beam displacements, whereas traditional variational formulations for beams and plates on half-space assume displacements as unknowns of the problem. The numerical model adopts Hermitian shape functions for the beam and piecewise constant function for the surface tractions. A set of numerical tests is performed for evaluating the effectiveness of the model in determining beam buckling loads and the corresponding modal shapes by varying the mechanical parameters characterizing the beam-substrate system and by considering the effect of beam length-to-width ratio. Several boundary conditions at beam ends are also taken into consideration. Numerical results are compared with existing analytical solutions, which are almost dedicated to beams with infinite length, with particular attention to critical load values and to buckling wavelength.

## 2. BASIC RELATIONSHIPS

### 2.1. Variational formulation

This work considers a slender elastic beam with length $L$ resting in bilateral and frictionless contact with a transversely isotropic semi-infinite half-space. The beam is referred to a Cartesian coordinate system (O; $x$, $y$, $z$), where the $x$–$y$ plane defines the half-space boundary, $x$ is assumed to be coincident with the centroidal axis of the beam, $z$ is chosen in the downward transverse direction and it is normal to the plane of isotropy of the half-space. The beam has a symmetric cross-section shape with respect to the axis $z$, with height $h$ and width $b$ representing the overall cross-section dimensions in $z$ and $y$ direction, respectively. Moreover, a flat cross-section base is considered, in order to define a rectangular contact area between the beam and the half-space with constant width $b$ and length $L$, allowing to introduce the dimensionless parameter $\chi = L/b$. The beam is loaded at its ends by a concentrated compressive force $P$ as shown in Fig. 1, where the simple case of beam rectangular cross-section is considered. A vertical load $p(x)$ distributed along the beam axis can also be applied to the beam. Following the assumptions already adopted for the beam on isotropic half-space subjected to static loads (Baraldi and Tullini, 2018), the beam experiences flexure only in $x$–$z$ plane, hence, together with the frictionless and bilateral conditions assumed between beam and substrate, only a vertical half-space traction $r(x, y)$ is acting upon the beam.

Focusing first on half-space behaviour, the three-dimensional problem for a homogeneous, linear elastic and transversely isotropic half-space loaded by a point force normal to its boundary plane has been studied by many authors, see (Michell, 1900; Liao and Wang, 1998; Kachanov et al., 2003; Ding et al., 2006; Anyaegbunam, 2014; Marmo et al., 2017; Argatov and Mishuris, 2018; Popov et al. 2019) and references cited therein. In particular, the vertical displacement *w* of a point on the half-space boundary due to a generic normal traction $r(x, y)$ is given by

$$w(x,y,0)=\frac{1}{\pi E_s}\int_{-b/2}^{b/2}\int_L \frac{r(\hat{x},\hat{y})\,\mathrm{d}\hat{x}\,\mathrm{d}\hat{y}}{d(x,y;\hat{x},\hat{y})} \tag{1}$$

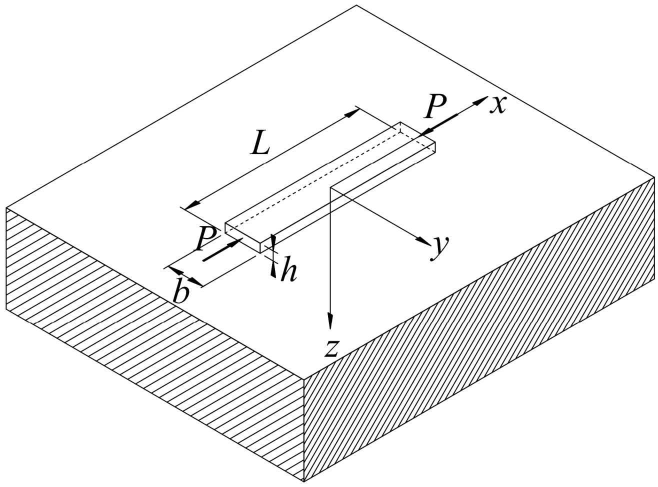


Fig. 1. Compressed beam resting on semi-infinite three-dimensional half-space.

where

$$d(x,y;\hat{x},\hat{y})=\sqrt{\left(x-\hat{x}\right)^2+\left(y-\hat{y}\right)^2} \tag{2}$$

is the distance between the points $(x, y, 0)$ and $(\hat{x}, \hat{y}, 0)$, and $E_s$ is the equivalent elastic moduli of the half-space along the vertical direction *z*. Details on such modulus can be found in the recent contribution by Baraldi and Tullini (2020) and in references cited therein. However, for an isotropic substrate, the equivalent elastic moduli $E_s$ reduces to $E_{\mathrm{soil}}/(1-\nu_{\mathrm{soil}}^2)$, where $E_{\mathrm{soil}}$ and $\nu_{\mathrm{soil}}$ are Young modulus and Poisson ratio of the isotropic substrate; correspondingly, Eq. (1) reduces to Boussinesq solution (Kachanov et al., 2003; Johnson, 1985).

Following the considerations done in Baraldi and Tullini (2018), due to the theorem of work and energy for exterior domains (Gurtin and Sternberg, 1961) and accounting for Eq. (1), the total potential energy of the half-space is

$$\Pi_s = -\frac{1}{2\pi E_s} \int_{-b/2}^{b/2} \int_L r(x, y)\, \mathrm{d}\, x\, \mathrm{d}\, y \int_{-b/2}^{b/2} \int_L \frac{r(\hat{x}, \hat{y})\, \mathrm{d}\, \hat{x}\, \mathrm{d}\, \hat{y}}{d(x, y; \hat{x}, \hat{y})} \tag{3}$$

Focusing on beam behaviour, an Euler-Bernoulli beam model is assumed, and restricting the analysis in the *x*-*z* plane, beam vertical displacement can be written as $w(x, y, z) = w(x)$. The total potential energy of the beam, including second order effects, can be written as

$$\Pi_b = \frac{1}{2} \int_L [D_b\, (w''(x))^2 - P(w'(x))^2]\, \mathrm{d}\, x - \int_L [(p(x) - \int_{-b/2}^{b/2} r(x, y)\, \mathrm{d}\, y)\, w(x)]\, \mathrm{d}\, x\,, \tag{4}$$

where prime denotes differentiation with respect to $x$ and $D_b = E_b\, J_b$, with $E_b$ being longitudinal elastic modulus and $J_b$ the second area moment of beam cross-section with respect to the $y$ axis.

Many constraint equations $R_i(w, w') = 0$ between displacements or rotations may be assigned along the beam axis. For example, a pinned-pinned beam requires the equation $w(L/2) - w(-L/2) = 0$. These constraint equations can be included in the total potential energy $\Pi$ of the beam-substrate system by means of a penalty approach. Hence, making use of Eqs. (3) and (4), the total potential energy of the beam-substrate system turns out to be (Reddy, 2006):

$$\Pi(w, r) = \Pi_b(w, r) + \Pi_s(r) + \frac{k}{2} \sum_i [R_i(w, w')]^2\,, \tag{5}$$

where $k$ is the penalty parameter, whose value should be large enough to satisfy the constraint equations accurately. It is worth noting that Boussinesq solution (1) holds for a half-plane loaded by surface tractions normal to its boundary, which must be free to deform elsewhere. The penalty approach allows to reformulate a problem with constraints as one without constraints.

Variational formulation analogous to Eq. (5) was obtained in (Kikuchi, 1980; Kikuchi and Oden, 1988; Bielak and Stephan, 1983) for beams resting on a Pasternak soil, in (Tullini and Tralli, 2010; Baraldi and Tullini, 2017) for beams and frames resting in bilateral frictionless contact with an elastic half-plane and in Baraldi and Tullini (2017) for a Timoshenko beam in bilateral frictionless contact with an elastic isotropic half-space. Moreover, mixed variational principle similar to Eq. (5) was used in Tullini et al. (2012) to study axially loaded thin structures perfectly bonded to an elastic substrate and in (Tullini et al., 2013a; Tullini et al., 2013b; Baraldi, 2019) to determine the buckling loads of beams in frictionless contact with an elastic half-plane and an elastic layer in plane state. Beams in perfect adhesion with an elastic half-plane are considered in (Tezzon et al., 2015; Tezzon et al., 2016). Differently with respect the proposed approach, traditional variational formulations are defined in terms of foundation displacements only (Selvadurai, 1979b; Selvadurai, 1980; Selvadurai, 1984).

Following the considerations already done in Baraldi and Tullini (2018), it must be pointed out that the beam model hypothesis implies vertical displacement $w$ varying only along $x$ direction and uniform vertical displacement along beam width. This hypothesis is satisfied if the beam cross-section is infinitely rigid with respect to the half-space in the $y$ direction, then the distribution of contact tractions $r$ in such direction is expected to be equal to the one generated by a rigid indenter with width $b$ in a plane strain problem (Johnson, 1985; Kachanov et al. 2003) and characterized by singularities close to section ends. However, uniform tractions $r$ along beam width are often taken into consideration when analytic solutions of infinite beams on elastic half-space are searched (Jiang et al., 2008, Tarasovs and Andersons, 2008), and the consequent non-uniform beam displacement along transversal direction is simplified by considering the displacement at beam centerline or an average value of transversal deflection. The two different approaches were investigated analytically for first by Biot (1937) for the static analysis of infinite beams and by Murthy (1973) for the corresponding stability analysis.

## 2.2 Discrete model

A simple discretization of the beam-substrate system can be created by subdividing the beam into FEs of equal length $l_{xi} = L/n_x$, where $n_x$ is the number of subdivisions in $x$ direction. The contact surface underneath the beam may be divided in $x$ direction with the same number of subdivisions assumed for the beam, whereas in $y$ direction, i.e. across the beam width, the number of subdivisions $n_y$ can be assumed larger than one in order to correctly modelling the non-uniform pressures generated by uniform displacements. In particular, for correctly describing reactions at contact surface edges with a small number of surface subdivisions, it is common to use power graded meshes (Erwin and Stephan, 1992; Graham and McLean, 2006), which are characterized by a grading exponent $\beta \geq 1$ that allows to obtain small subdivisions close to surface edges. The same type of power graded discretization can be also adopted in $x$ direction close to beam ends, in order to obtain small subdivisions at the corners of the foundation. However, the convergence tests already done by authors with the static case (Tullini et al., 2013a) showed that this type of mesh refinement does not influence significantly the accuracy of numerical results, hence, it will not be adopted in this work. Then, a piecewise constant discretization of contact surface tractions is adopted by assuming constant shape functions, whereas classical Hermitian polynomials are assumed as beam shape functions (Reddy, 2006).

The stationarity condition of the total potential energy $\Pi(w, r)$ written in discrete form provides the following system:

$$\begin{bmatrix} \frac{D_b}{L^3}\left(\tilde{\mathbf{K}}_b - \frac{PL^2}{D_b}\tilde{\mathbf{K}}_g\right) & b\tilde{\mathbf{H}} \\ b\tilde{\mathbf{H}}^{\mathrm{T}} & -\frac{b}{E_s}\tilde{\mathbf{G}} \end{bmatrix} \begin{Bmatrix} \mathbf{q} \\ \mathbf{r} \end{Bmatrix} = \begin{Bmatrix} \mathbf{F} \\ \mathbf{0} \end{Bmatrix}, \qquad (6)$$

where the vector $\mathbf{q}$ collects beam nodal displacements, $\mathbf{r}$ denotes the vector of the constant soil reactions, $\mathbf{F}$ is the vector of the external loads, $D_b/L^3\,\tilde{\mathbf{K}}_b$ is the elastic stiffness matrix of the beam, $P/L\,\tilde{\mathbf{K}}_g$ is the geometric (or incremental) stiffness matrix (Reddy, 2006; Tullini et al., 2013a), and the elements of the matrices $\tilde{\mathbf{H}}$ and $\tilde{\mathbf{G}}$ are reported in Baraldi and Tullini (2018). The system in Eq. (6) yields the following solution

$$\mathbf{r} = E_s\tilde{\mathbf{G}}^{-1}\tilde{\mathbf{H}}^{\mathrm{T}}\mathbf{q}, \qquad (7)$$

$$[\tilde{\mathbf{K}}_b - \lambda\tilde{\mathbf{K}}_g + (\alpha L)^3 \tilde{\mathbf{K}}_{\text{soil}}]\mathbf{q} = \frac{L^3}{D_b}\mathbf{F}, \tag{8}$$

where $\tilde{\mathbf{K}}_{\text{soil}}$ is the stiffness matrix of the soil or three-dimensional half-space

$$\tilde{\mathbf{K}}_{\text{soil}} = \tilde{\mathbf{H}}\tilde{\mathbf{G}}^{-1}\tilde{\mathbf{H}}^{\text{T}}, \tag{9}$$

the axial load multiplier is $\lambda = PL^2/D_b$, and $\alpha L$ is the well-known (Biot, 1937; Vesic, 1961; Selvadurai, 1979a; Baraldi and Tullini, 2018) parameter characterizing the soil-foundation system:

$$\alpha L = \sqrt[3]{\frac{E_s\, b\, L^3}{D_b}}. \tag{10}$$

The adopted mixed finite element is particularly simple and effective, as shown in Baraldi and Tullini (2018) for the static case, where the numerical properties of the proposed FE model are also discussed. With regard to the determination of critical load $P_{\text{cr}}$, a homogeneous system associated to Eq. (8) must be considered and the buckling loads are given by the roots $\lambda_{\text{cr}}$ of the equation $\det[\tilde{\mathbf{K}}_b - \lambda\tilde{\mathbf{K}}_g + (\alpha L)^3 \tilde{\mathbf{K}}_{\text{soil}}] = 0$, which can be suitably reduced to a standard eigenvalue problem. Introducing the definition of Euler critical load:

$$P_{\text{cr,E}} = \frac{\pi^2 D_b}{L^2}, \tag{11}$$

the dimensionless buckling loads turn out to be given by $P_{\text{cr}}/P_{\text{cr,E}} = \lambda_{\text{cr}}/\pi^2$.

## 3. NUMERICAL TESTS

The buckling of Euler-Bernoulli beams with finite length is investigated by assuming three different boundary conditions at beam ends, following the same approach adopted for the beam on elastic half-plane (Tullini et al., 2013a). However, a preliminary convergence test is performed by determining the first three critical loads of a beam with free ends assuming two $\alpha L$ and $\chi$ values, for increasing beam subdivisions and by considering several contact surface discretization types along beam width. Then, assuming a beam with aspect ratio $\chi = 10$, critical loads and modal shapes are determined for increasing $\alpha L$. Finally, several considerations are done varying parameter $\chi$.

### 3.1. Convergence test

The first three critical loads of a compressed beam with free ends on half-space are determined by considering four different geometrical and mechanical conditions represented by the parameters $\alpha L$ equal to 5 and 25 and $\chi$ equal to 10 and 100. Numerical reference solutions $P^{ref}_{\mathrm{cr},f,i}$, with $i = 1, 2, 3$, are determined by assuming $n_x = 2^{11}$ and a $n_y = 7$ with a power-graded discretization with $\beta = 3$ (Tab. 1); then, the influence of the approximation of contact tractions along beam width is evaluated by considering the simple case with $n_y = 1$, namely a constant traction along beam width, and the more accurate case with a power-graded subdivision with $n_y = 3$ and $\beta = 3$. Fig. 2 shows the relative differences $\delta P_{\mathrm{cr},f,i} = (P^{ref}_{\mathrm{cr},f,i} - P_{\mathrm{cr},f,i}) / P^{ref}_{\mathrm{cr},f,i}$ obtained with the two proposed discretization types for increasing $n_x$. Differences turn out to have the same behaviour of those determined for the static case in terms of maximum vertical displacement and contact traction, since they tend to nonzero values instead of tending to zero. In general, the critical loads obtained with $n_y = 3$ are quite close to reference solutions and differences generally tend to be less than 1% for $n_x > 2^7$ with $\alpha L = 5$ and $n_x > 2^8$ with $\alpha L = 25$; in particular, with $\alpha L = 25$, differences obtained for 1st and 2nd critical loads, which are coincident, start to converge for $n_x > 2^7$, with values close to 0.4% with $\chi = 10$ and 0.2% with $\chi = 100$, highlighting that long beams on stiff half-space are less influenced by the subdivision refinement along $x$ direction. The critical loads obtained with $n_y = 1$ turn out to be less accurate with respect to reference solutions and differences are never less than 1% in the four cases considered. Convergence tests show that $\alpha L$ parameter slightly influence the accuracy of the results, with a better convergence obtained with $\alpha L = 25$, whereas the differences obtained with $\chi = 100$ are slightly smaller than those obtained with $\chi = 10$, highlighting the necessity of a more accurate contact surface discretization in case of a short beam or a beam with a small length-to-width ratio.

However, the order of magnitude of differences obtained with $n_y = 1$ is still acceptable for performing the upcoming numerical tests, since differences are generally less than 5% with $n_x > 2^7$. In the following numerical test, the buckling loads are determined by assuming $n_x = 2^7$ and $n_y = 3$ with a power-graded discretization with β = 3.

It is worth noting that the critical loads determined by assuming constant tractions along beam width turn out to be smaller than those obtained both with a less and more accurate contact surface discretization along beam width. This aspect is in agreement with the results obtained by Murthy (1973) for the stability of beams with infinite length, since critical loads obtained with uniform reactions across beam width and assuming beam deflections along its longitudinal axis turned out to be smaller than critical loads obtained with a reaction profile across beam width same as that of a rigid stamp.

| $P^{ref}_{cr,f,i}/[P_{cr,E}(\alpha L)^2]$ | $\alpha L = 5$ | | $\alpha L = 25$ | |
|---|---|---|---|---|
| | $\chi = 10$ | $\chi = 100$ | $\chi = 10$ | $\chi = 100$ |
| 1 | 0.1312 | 0.3088 | 0.1040 | 0.1809 |
| 2 | 0.1731 | 0.3262 | 0.1040 | 0.1809 |
| 3 | 0.4050 | 0.6785 | 0.1641 | 0.3130 |

Tab. 1. Reference critical loads for a compressed beam with free ends on elastic half-space, obtained with $n_x = 2^{11}$ and a power-graded subdivision along y direction with $n_y = 7$ and β= 3.

(a) 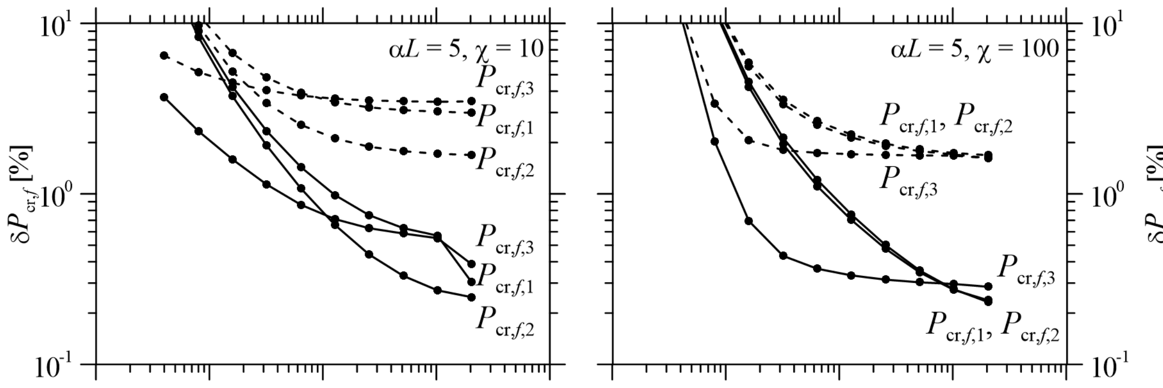 (c)

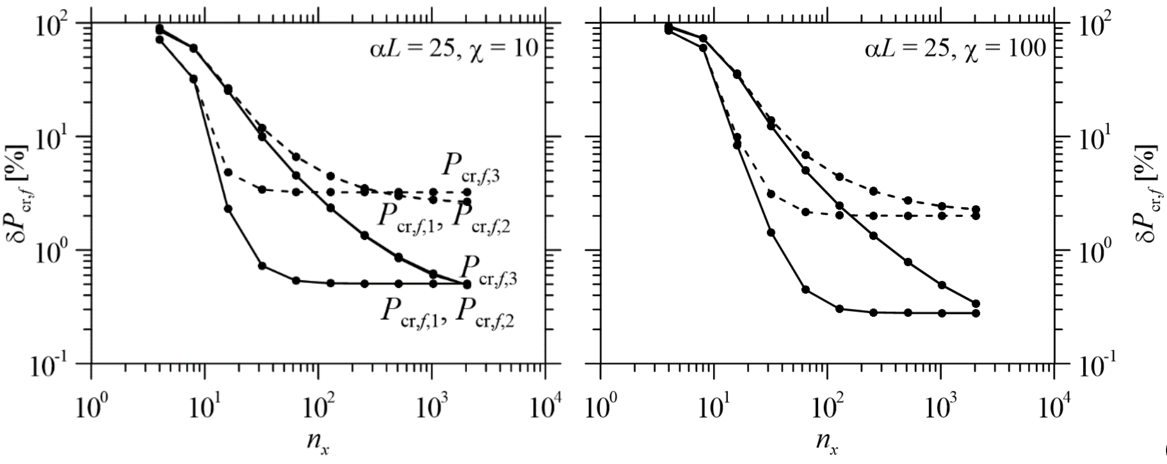


(b) (d)

Fig. 2. Relative differences for the first three critical loads versus the overall number of subdivisions along beam length for a compressed beam with free ends with $\alpha L = 5$ (a, c) and 25 (b, d), with $\chi = 10$ (a, b) and $\chi = 100$ (c, d). Results obtained with $n_y = 1$ (dashed lines) and $n_y = 3$ (continuous lines), assuming results in Tab. 1 as reference.

### 3.2. Beam of finite length with sliding ends

The buckling of a beam with sliding ends on elastic half-space, with $\chi = 10$, is considered. This case may refer to a frame with rigid columns and simply supported beams; thus, the structure prevents rotations at the ends of the foundation beam but allows independent vertical displacements. The constraint equations to be used in Eq. (5) are $R_1 = w'(L/2) - w'(-L/2) = 0$ and $R_2 = w'(L/2) + w'(-L/2) = 0$. Assuming a penalty parameter $k = 10^9\, l_i\, D_b/L^3$ that ensures a stable numerical solution of Eq. (8), Fig. 3a shows dimensionless critical loads $P_{cr,s}/P_{cr,E}$ varying with $\alpha L$. The numerical results show a behaviour analogous to the same beam type on an elastic half-plane, since critical loads increase for increasing $\alpha L$ and present crossing points and curve veering. It is worth noting that, for $\alpha L$ equal to zero, critical loads are equal to the values $P_{cr,m}(0)/P_{cr,E} = m^2$, with $m = 1, 2, 3\ldots$, typical of a beam with pinned or sliding ends without a supporting medium. Fig. 3b shows the ratio $P_{cr,s}/[P_{cr,E}\ (\alpha L)^2]$ versus the parameter $\alpha L$. For increasing $\alpha L$, the ratios corresponding to the first eigenvalue do not converge to a stable value, whereas in case of a beam on elastic half-plane such convergence was evident and the corresponding critical load was equal to that of a beam with infinite length (Tullini et al., 2013a). However, for α*L* equal to 50, the critical load is close to

$$P_{\mathrm{cr},s} = 0.143\, P_{\mathrm{cr,E}} (\alpha L)^2 \,. \tag{12}$$

This result will be further investigated in the final part of the manuscript by evaluating the influence of χ on critical load values and by evaluating their relationship with respect to the critical loads of a beam on elastic half-plane.

Fig. 4 shows first and second mode shapes of the beam with sliding ends for two α*L* values. Mode shapes are analogous to those of a beam with sliding ends on elastic half-plane, since they are sinusoidal and characterized by an increasing number of half-waves for increasing α*L*.

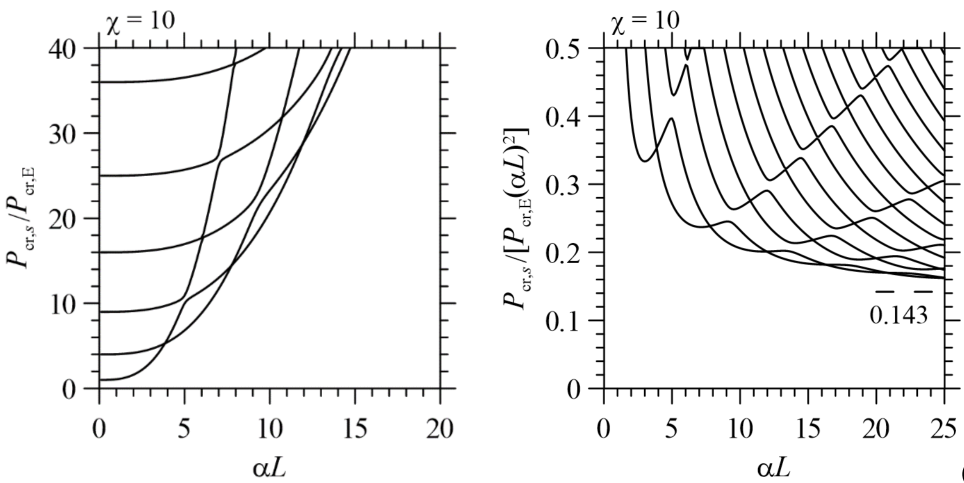


(a) (b)

Fig. 3. Dimensionless critical loads $P_{\mathrm{cr},s}$ versus α*L* for a beam with sliding ends on elastic half-space.

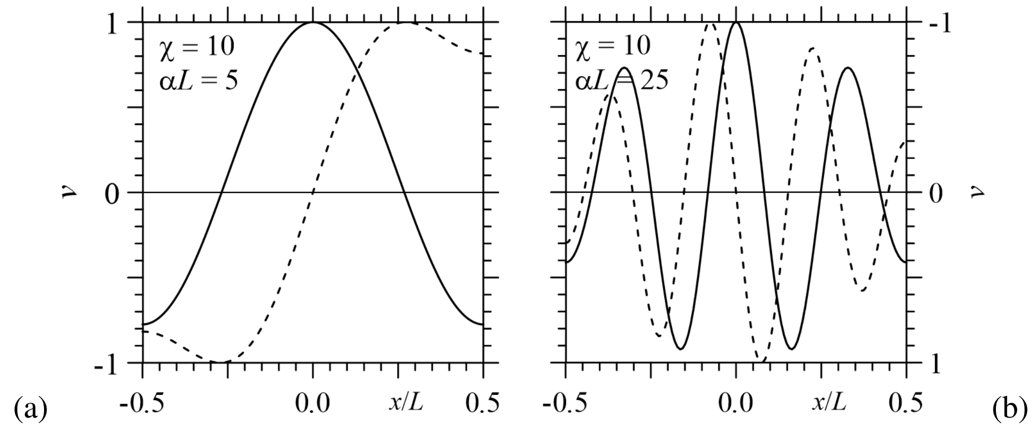


Fig. 4. First (continuous line) and second (dashed line) mode shapes for a beam with sliding ends and $\alpha L$ equal to 5 (a) and 25 (b).

### 3.3. Beam of finite length with pinned ends

The case of a foundation beam with pinned ends may refer to a rigid frame whose columns are hinged to the foundation beam; thus, the structure enforces zero relative displacement at the beam ends, but allows independent rotations. The constraint equation to be applied to Eq. (5) is $R_1 = w(L/2) - w(-L/2) = 0$. Assuming a penalty parameter $k = 10^6 D_b/L^3$, Fig. 5a shows dimensionless critical loads $P_{cr,p}/P_{cr,E}$ are versus $\alpha L$. For $\alpha L$ equal to zero, critical loads converge to the values already highlighted in the previous subsection $P_{cr,m}(0)/P_{cr,E} = m^2$, with $m$ = 1, 2, 3…, typical of a beam with pinned ends without any other support. Critical loads increase for increasing $\alpha L$ and present crossing points and curve veering, however the first critical load appears quite far from other results, whereas second critical load is quite close to the third and fourth ones, differently with respect to the beam with pinned ends on elastic half-plane.

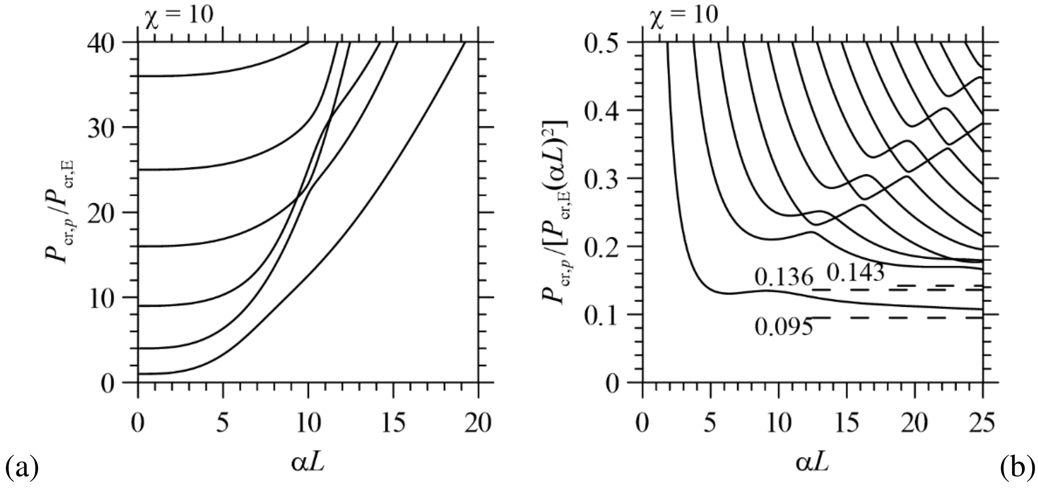


Fig. 5. Dimensionless critical loads $P_{cr,p}$ versus $\alpha L$ for a beam with pinned ends on half-space.

Considering Fig. 5b showing the ratio $P_{cr,p}/[P_{cr,E}\ (\alpha L)^2]$ versus the parameter $\alpha L$, numerical results do not show a convergence to stable values, however, for $\alpha L$ equal to 50, the first critical load is equal to:

$$P_{cr,p,1} = 0.095\,P_{cr,E}(\alpha L)^2\,, \tag{13}$$

whereas the second critical load is equal to:

$$P_{cr,p,2} = 0.136\,P_{cr,E}(\alpha L)^2\,, \tag{14}$$

which is slightly smaller but quite close to Eq. (12). Such a value is reached by the third and fourth critical loads for increasing $\alpha L$:

$$P_{cr,p,3} = P_{cr,p,4} = P_{cr,s} = 0.143\ P_{cr,E}\ (\alpha L)^2 \tag{15}$$

Furthermore, $P_{cr,p,2}$ is 95% of $P_{cr,s}$, this ratio is larger than the corresponding one obtained for the beam on elastic half plane (Tullini et al., 2013a) (0.106 / 0.121 = 88%).

Fig. 6 shows first and second mode shapes for several $\alpha L$ values. For $\alpha L = 5$ (Fig. 6a), first and second mode shapes are sinusoidal, whereas for $\alpha L = 10$ (Fig. 6b), first and second mode shapes can not be described by sinusoidal functions, similarly to the case of a beam with pinned ends on elastic half-plane. For $\alpha L = 25$ (Fig. 6c), the first mode shape is characterized by large deflections at beam ends, but the second mode shape is sinusoidal. Increasing $\alpha L$ (Fig. 6d), the first mode shape has the same behaviour found for the beam with pinned ends on elastic half-plane, characterized by large deflections at beam ends and negligible displacements near beam midpoint, whereas the second mode shape is characterized by large deflections at beam ends and sinusoidal deflections not negligible along its length. This behaviour may justify the corresponding critical load (Eq. 14), which is quite close to the third and fourth critical loads and to Eq. (12), which are typical of sinusoidal mode shapes.

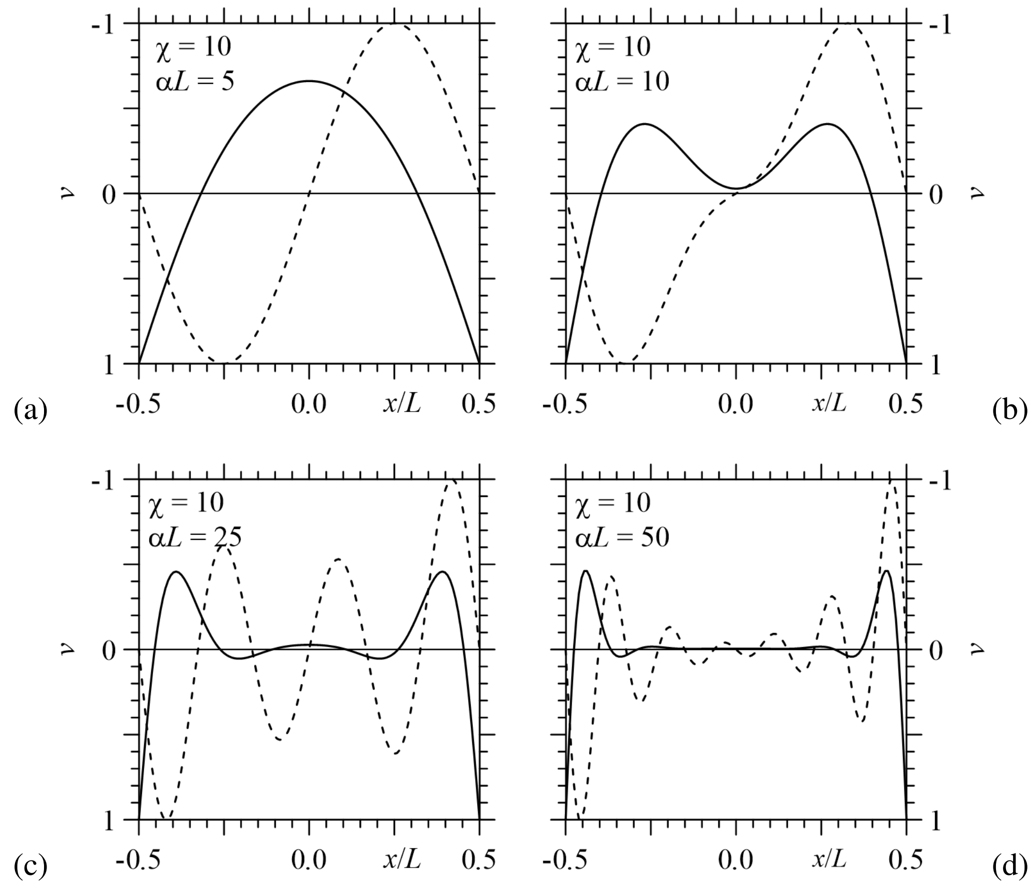


Fig. 6. First (continuous line) and second (dashed line) mode shapes for a beam with pinned ends on half-space and $\alpha L$ equal to 5 (a), 10 (b), 25 (c) and 50 (d).

### 3.4. Beam of finite length with free ends

The buckling of a beam with free ends on elastic half-space is finally considered. In Fig. 7a, the dimensionless critical loads $P_{cr,f}/P_{cr,E}$ are plotted versus $\alpha L$, whereas Fig. 7b shows the ratio $P_{cr,f}/[P_{cr,E}\,(\alpha L)^2]$ versus the parameter $\alpha L$. Critical loads increase for increasing $\alpha L$ and present crossing points and curve veering. First and second critical loads, which are separated with respect to other results, present some crossing points and both converge to the value given in Eq. 13 for α*L* = 50, whereas the third and fourth eigenvalues converge to Eq. 12.

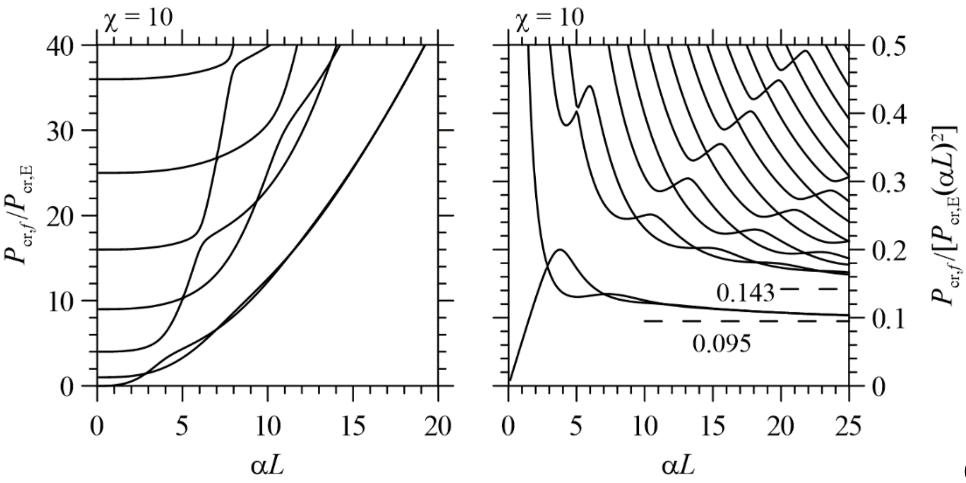


(a) (b)

Fig. 7. Dimensionless critical loads $P_{\mathrm{cr},f}$ versus α*L* for a beam with free ends on half-space.

Fig. 8 shows first and second mode shapes for increasing α*L*. Analogously to the case of the beam with free ends on elastic half-plane, for α*L* = 1 (Fig. 8a) the first mode shape represents a rigid body rotation and the corresponding critical load tends to zero, whereas the second mode shape is sinusoidal. For α*L* = 5 (Fig. 8b), after the first intersection point between first and second critical load curves, the fist mode shape is sinusoidal, but the second one is antisymmetric and characterized by large displacements at beam ends. Increasing α*L* (Figs. 8c and 8d), both mode shapes are characterized by large displacements at beam ends and negligible deformations close to beam midpoint. The symmetric mode shapes presented in Figs. 8a-d turn out to be coincident with the first mode shape obtained for the beam with pinned ends.

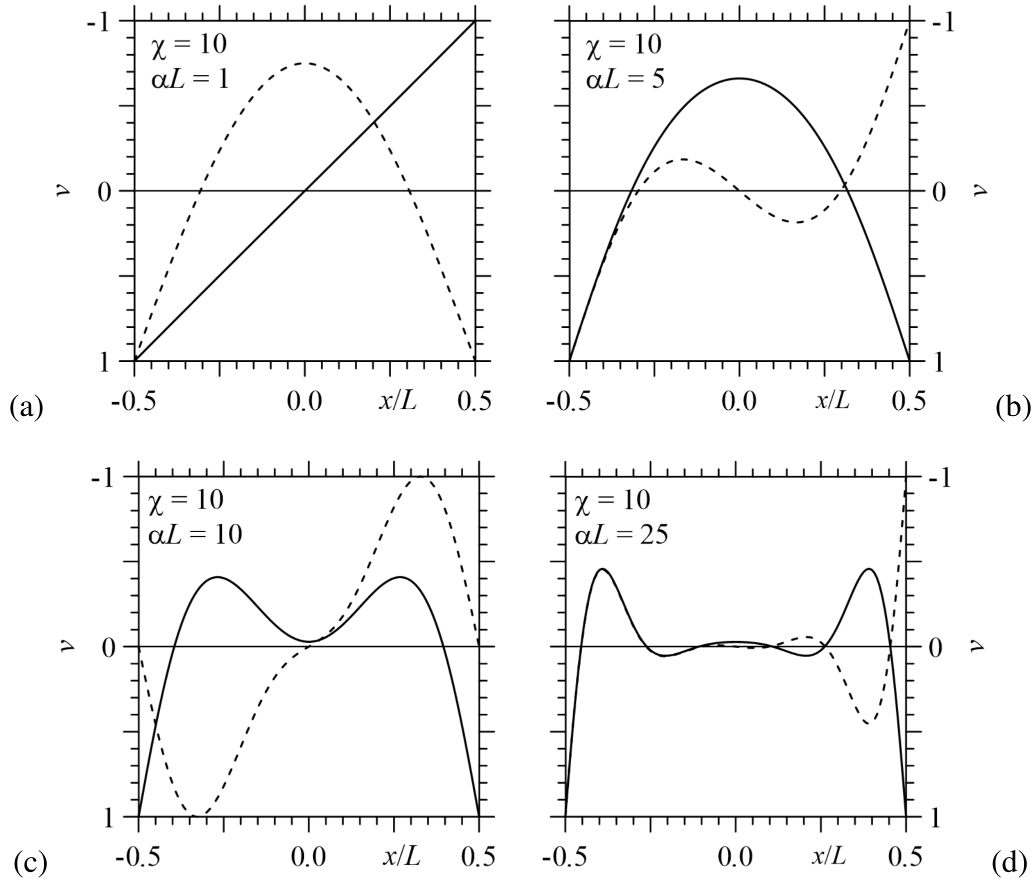


Fig. 8. First (continuous line) and second (dashed line) mode shapes for a beam with free ends and $\alpha L$ equal to 1 (a), 5 (b), 10 (c) and 25 (d).

## 4. INFLUENCE OF BEAM WIDTH ON OVERALL BEAM BUCKLING

The numerical tests performed in the previous section are characterized by beam length-to-width ratio $\chi = 10$. Further numerical tests can demonstrate that the buckling of a beam with a generic $\chi$ ratio on a three-dimensional half-space always follows the behaviour of any beam on an elastic support. However, the critical load values presented in Eqs. (12), (13) and (14), obtained with beams on a stiff soil ($\alpha L = 50$), strictly depend on $\chi$. Further values of $P_{cr,p,1}/[P_{cr,E}\,(\alpha L)^2]$, $P_{cr,p,2}/[P_{cr,E}\,(\alpha L)^2]$, and $P_{cr,s}/[P_{cr,E}\,(\alpha L)^2] = P_{cr,p,3}/[P_{cr,E}\,(\alpha L)^2]$ with $\alpha L = 50$ and varying $\chi$ are collected in Tab.2.

| | 2D Tullini et al., 2013a | $\chi = L/b$ | | | | | | | | |
|---|---|---|---|---|---|---|---|---|---|---|
| | | 0.1 | 1 | 2 | 3 | 4 | 5 | 10 | 50 | 100 |
| | | | | | | | | | | |
| $P_{cr,p,1}/[P_{cr,E}\ (\alpha L)^2]$ | 0.083 | 0.083 | 0.084 | 0.086 | 0.087 | 0.088 | 0.089 | 0.095 | 0.124 | 0.147 |
| $P_{cr,p,2}/[P_{cr,E}\ (\alpha L)^2]$ | 0.106 | 0.107 | 0.112 | 0.115 | 0.119 | 0.122 | 0.125 | 0.136 | 0.194 | 0.240 |
| $P_{cr,s}/[P_{cr,E}\ (\alpha L)^2]$ | 0.121 | 0.122 | 0.124 | 0.126 | 0.128 | 0.130 | 0.133 | 0.143 | 0.199 | 0.244 |

Tab. 2 – Dimensionless critical loads of a beam on half-space with $\alpha L = 50$ varying $\chi$.

Dimensionless critical loads increase for increasing $\chi$; moreover, the second dimensionless critical load tends to be more and more close to the third one increasing $\chi$. For example, for $\chi = 1$ the ratio between $P_{cr,p,2}$ and $P_{cr,s}$ is close to 0.9, whereas for $\chi = 100$ the same ratio is close to 0.98. Fig. 9 shows the first three dimensionless critical loads of a beam on half-space, namely $P_{cr,p,1}$ (plus symbols), $P_{cr,p,2}$ (circles), and $P_{cr,p,3} = P_{cr,s}$ (crosses) for increasing $\alpha L/\chi = \alpha b$ by considering several $\alpha L$ and $\chi$ combinations.

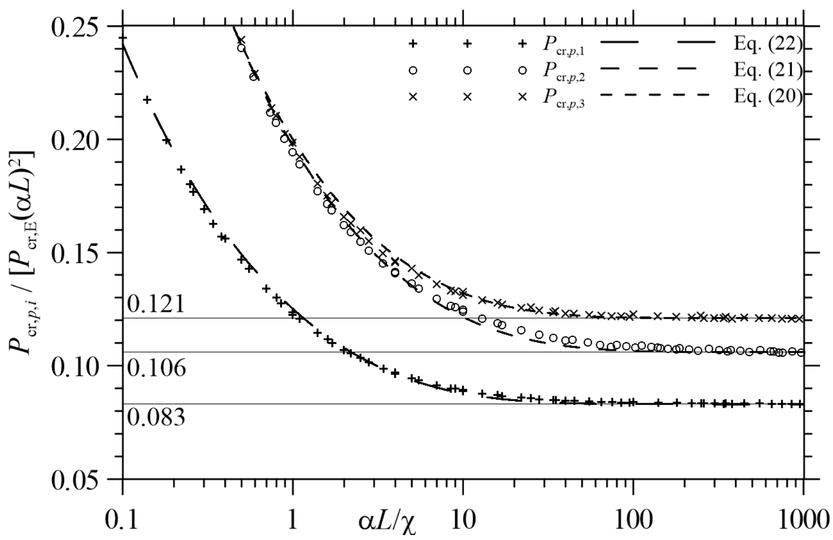

Fig. 9. First three dimensionless critical loads of a beam on half-space versus $\alpha L/\chi$.

It is worth noting that for small $\chi$ values, $\alpha L/\chi$ increases and the beam has a very short length with respect to its width. However, buckling modes along beam width are not allowed by the proposed model, since deformations along beam width are neglected; hence, the case of a beam having a large width with respect to its length numerically converges to a plane strain condition. In fact, for $\chi$ tending to zero or $\alpha b$ tending to infinite, dimensionless critical loads $P_{\mathrm{cr},p,i}$ for $i$ = 1, 2 3, turn out to converge to the corresponding ones obtained for the beam on elastic half plane (Tullini et al., 2013a) (continuous lines in Fig. 9):

$$P^{\mathrm{2D}}_{\mathrm{cr},p,1} = 0.083\, P_{\mathrm{cr,E}}\, (\alpha L)^2\,, \tag{16}$$

$$P^{\mathrm{2D}}_{\mathrm{cr},p,2} = 0.106\, P_{\mathrm{cr,E}}\, (\alpha L)^2\,, \tag{17}$$

$$P^{\mathrm{2D}}_{\mathrm{cr},p,3} = P^{\mathrm{2D}}_{\mathrm{cr},s} = 0.121\, P_{\mathrm{cr,E}}\, (\alpha L)^2 = 3/(2^{4/3}\pi^2) P_{\mathrm{cr,E}}\, (\alpha L)^2\,. \tag{18}$$

Nonetheless, in the plane strain state, the parameter $\alpha L$ contains the ratio $E_b/(1-\nu_b^2)$, where $\nu_b$ is the Poisson ratio of the beam, instead of the beam modulus $E_b$, as in a plane stress state.

Eq. (18) allows evaluation of the critical strain in a form frequently used in the design of structural sandwich panels (Allen, 1969; Ley et al., 1999; Davies, 2001) and in flexible and stretchable electronics (Huang, 2005; Genzer and Groenewold, 2006; Jiang et al., 2008):

$$e^{\mathrm{2D}}_{\mathrm{cr},s} = \frac{P^{\mathrm{2D}}_{\mathrm{cr},s,1}}{E_b\, b\, h} = 0.52 \left( \frac{E_s}{E_b} \right)^{2/3}\,. \tag{19}$$

In order to fit numerical results and obtaining approximated functions for the first three dimensionless critical loads of a beam on elastic half-space, the following expressions are proposed and added with dashed lines to Fig. 9:

$$P_{\mathrm{cr},p,1} / [P_{\mathrm{cr,E}}\, (\alpha L)^2] = 0.083 \coth[0.80\, (\alpha b)^{0.35}]\,, \tag{20}$$

$$P_{\mathrm{cr},p,2} / [P_{\mathrm{cr,E}}\, (\alpha L)^2] = 0.106 \coth[0.60\, (\alpha b)^{0.35}]\,, \tag{21}$$

$$P_{\mathrm{cr},s} / [P_{\mathrm{cr,E}} (\alpha L)^2] = 0.121 \coth[0.70 (\alpha b)^{0.35}] . \quad (22)$$

For increasing $\alpha b$ the proposed approximated expressions converge to the numerical results of a beam on elastic half-plane and are characterized by determination factor $R^2$ close to 1, in particular for all $\alpha b$ values with Eq. (22) and for $\alpha b < 10$ with Eqs. (20) and (21).

Numerical results in Fig. 9 also show that $P_{\mathrm{cr},p,2}$ and $P_{\mathrm{cr},s}$ turn out to be coincident for decreasing $\alpha b$ or increasing $\chi$. This aspect is justified by the mode shapes corresponding to $P_{\mathrm{cr},p,2}$ obtained with large $\alpha L$ values, already shown with dashed lines in Figs. 6c and 6d, and characterized by sinusoidal deflections with large amplitude close to beam ends. Analogous sinusoidal displacements are shown in Fig. 10 for $\alpha L = 50$ and increasing $\chi$, hence decreasing $\alpha b$. Large beam deflections are located close to beam ends in all the cases considered, but beam displacements along beam length increase and tend to become sinusoidal for increasing $\chi$. In particular, Figs. 10e and 10f show that beam deflections are sinusoidal with different amplitude along beam length and wavelength appears to be uniform. These modal shapes are quite similar to those of a beam with sliding ends (Fig. 4b) and the corresponding wavelengths are investigated in the next sub-section.

It is worth noting that the buckling behaviour of a beam with pinned ends on half-space turns out to be quite similar to that of the same beam on Winkler substrate (Hetenyi, 1946), which is characterized by the second critical load converging to the same value of the third and fourth ones, with a sinusoidal modal shape over the entire beam length.

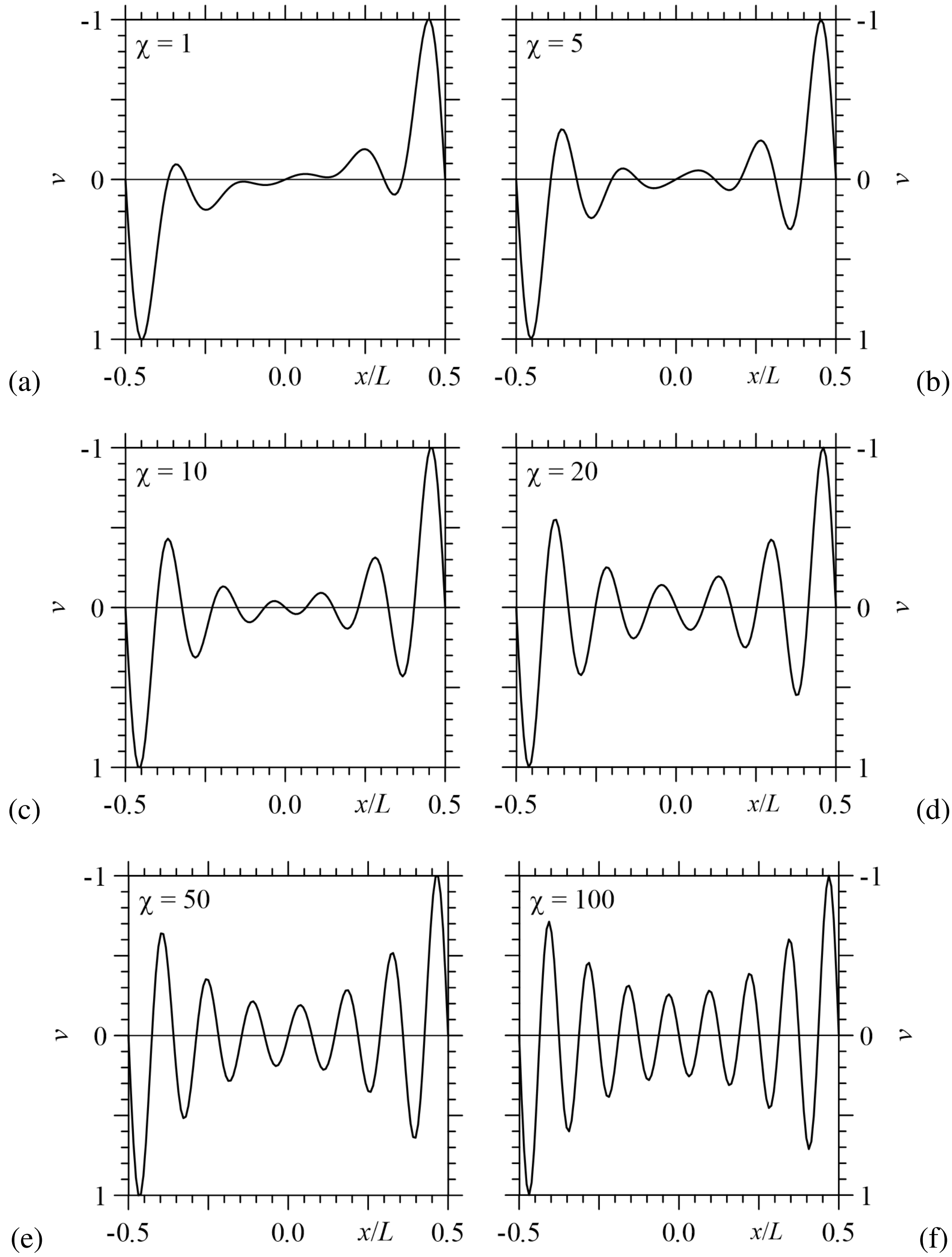


Fig. 10. Second mode shape for a beam with pinned ends, $\alpha L$ = 50 and increasing $\chi$.

## 4.1 Influence of beam width on buckling wavelength

As stated into the introduction, the determination of buckling wavelength and amplitude of thin films on elastic substrates is important for stretchable and flexible electronics. Hence, the proposed numerical model is adopted for determining the critical buckling wavelength $\Lambda_{cr}$ corresponding to

$P_{cr,s}$ for varying $\alpha L$ and $\chi$. In order to avoid the local effect of the sliding ends, $\Lambda_{cr}$ is evaluated numerically as the average wavelength of the sinusoidal modal shape for $-L/4 \le x \le L/4$ (Fig. 11).

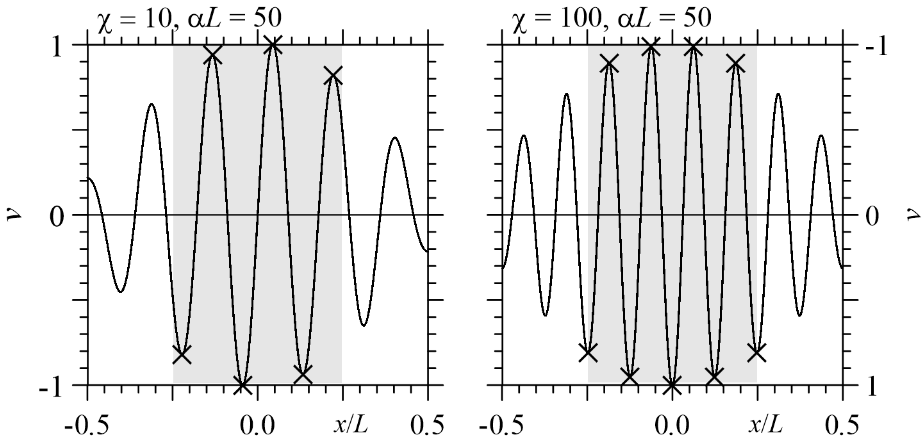


(a) (b)

Fig. 11. Determination of buckling wavelength corresponding to the minimum critical load for $-L/4 \le x \le L/4$, for two $\alpha L$ and $\chi$ cases.

Results are collected in Fig. 12a with cross symbols for several $\chi$ values. The buckling wavelength $\Lambda_{cr}$ for each length-to-width ratio $\chi$ turns out to decrease for increasing $\alpha L$ and it decreases for increasing $\chi$. However, for decreasing $\chi$, $\Lambda_{cr}$ values turn out to be close to those of a beam on elastic half-plane $\Lambda_{cr,2D}$ (dashed line in Fig. 12a). It is worth noting that $\Lambda_{cr,2D} = 9.97/\alpha = 2^{5/3}\pi/\alpha$; such expression can be derived analytically from Reissner (1937) formulation, it was highlighted in Volynskii et al. (2000) and it was already obtained numerically by authors for a beam with sliding ends on elastic half-plane (Tullini et al., 2013a).

In order to obtain an approximated expression for $\Lambda_{cr}$, it is useful to introduce a function $f(\alpha L/\chi) = f(\alpha b)$, representing the ratio between the buckling wavelength of a beam on elastic half-space and the buckling wavelength of a beam on elastic half-plane:

$$\Lambda_{cr} = \Lambda_{cr,2D}\, f(\alpha L/\chi) \tag{23}$$

Ratios $\Lambda_{cr} / \Lambda_{cr,2D}$ obtained numerically with the proposed model are shown in Fig. 12b versus $\alpha b$ with cross symbols. It can be observed that the buckling wavelength values obtained with $\alpha b$ larger than $10^3$ converge to those of a beam on elastic half-plane, since the corresponding ratios $\Lambda_{cr} / \Lambda_{cr,2D}$ converge to 1. A good approximation of the numerical results is given by the following expression:

$$f(\alpha L, \chi) = f(\alpha b) = \tanh[0.88(\alpha b)^{0.25}], \tag{24}$$

which is added with a continuous line to Fig. 12b versus $\alpha b$. Then, the approximated expression for the wavelength of beams on elastic substrate is:

$$\Lambda_{cr} = \Lambda_{cr,2D} \tanh[0.88(\alpha b)^{0.25}], \tag{25}$$

which turns out to be similar, but not coincident, with that of a beam with infinite length on half-space proposed by Jiang et al. (2008), which is in better agreement with their experimental results (circles in Fig. 12b, error bars with plus symbols). The approximated expression for $\Lambda_{cr}$ is characterized by a coefficient of determination $R^2$ close to 1 for almost all $\alpha L$ and $\chi$ combinations, with the smallest $R^2 = 0.77$ obtained with a beam having $\chi = 100$ and varying $\alpha L$ from 50 to 1000. It is worth noting that the convergence of Eq. (24), for increasing $\alpha b$, to the analytical solution typical of the plane state case, allows to consider such equation as a generalized approximated expression for the critical wavelength of beams on an elastic continuum. It is worth noting that Euler-Bernoulli beam model holds for sufficiently high values of the critical half-wavelength, for example, $\Lambda_{cr}/2 > 10\,h$. Thus, making use of Eq. (25), the inequality $\alpha h < f(\alpha b)/2$ holds. For beam with $\alpha h > f(\alpha b)/2$, the transverse shear deformation of the beam may become important and needs to be considered. For the experimental data reported by Jiang et al. (2008), a Euler-Bernoulli beam model may be adopted.

Finally, the buckling wavelength values of the modal shapes corresponding to $P_{cr,p,2}$ (Fig. 10), determined with the approach highlighted in Fig. 11 and compared with $\Lambda_{cr,2D}$, are shown in Fig. 13 for relatively small $\alpha b$ values, being in good agreement with Eq. (24) and justifying the convergence of $P_{cr,p,2}$ to $P_{cr,s}$ for decreasing $\alpha b$.

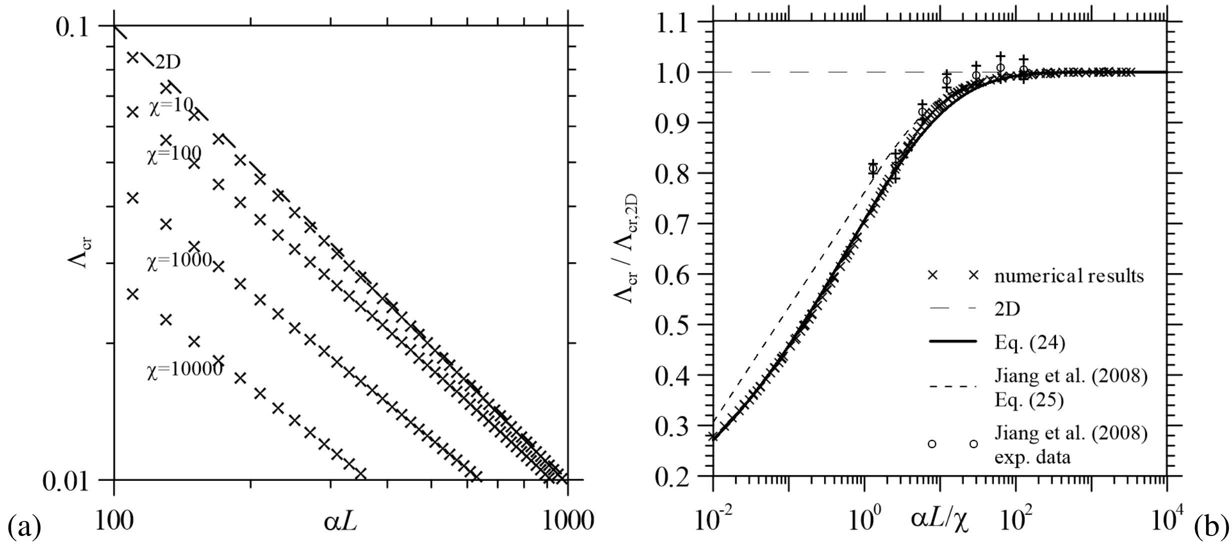


Fig. 12. Buckling wavelength of beams with sliding ends on elastic half-space versus $\alpha L$ and varying $\chi$ (a); with respect to the wavelength of a beam on elastic half-plane versus $\alpha L/\chi$ (b).

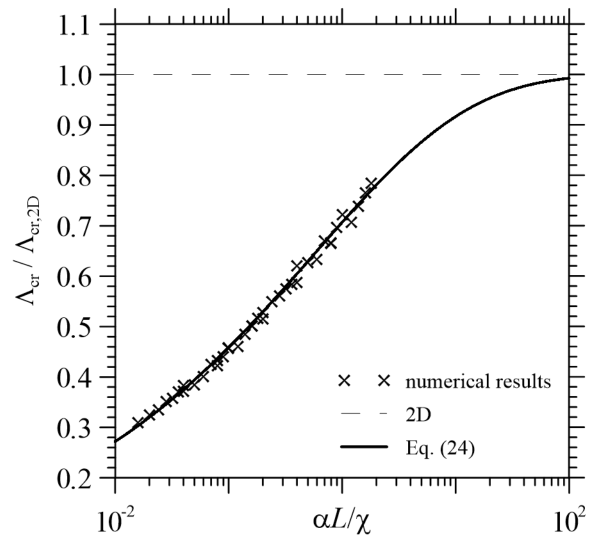


Fig. 13. Buckling wavelength corresponding to $P_{cr,p,2}$ with respect to the wavelength of a beam on elastic half-plane versus $\alpha L/\chi$.

## CONCLUSIONS

A simple and effective FE-BIE coupling method for beams on three-dimensional half-space, already investigated by authors by performing static analyses (Baraldi and Tullini, 2018), was here applied to buckling problems of slender beams and coatings having finite width and length, in bilateral and frictionless contact with an elastic half-space. Several beam end constraints were taken into consideration for simulating free coatings or different superstructures connected to a foundation beam. The proposed coupled FE-BIE model turned out to be fast and effective in evaluating beam buckling loads and the corresponding modal shape characteristics.

Considering a fixed beam length-to-width ratio $\chi$ equal to 10, the buckling behaviour of a beam on elastic half-space turned out to be similar to that of a beam on elastic half-plane. On one hand, the proposed numerical tests showed a convergence, for low values of $\alpha L$, to the critical loads of beams without an elastic support. On the other hand, for increasing beam slenderness and/or substrate stiffness, a variation of the critical loads proportional to $(\alpha L)^2$ was found, but dimensionless minimum critical loads were slightly larger than the corresponding ones typical of a beam on elastic half-plane (Tullini et al., 2013a). Furthermore, the beam with sliding ends showed a behaviour characterized by sinusoidal modal shapes over its length, which is typical of a beam with infinite length. The first and second dimensionless critical loads of the beam with pinned ends turned out to be slightly smaller than that obtained with the beam with sliding ends and the corresponding modal shapes were characterized by large amplitudes close to beam ends, whereas the third critical load converged to that of the beam with sliding ends, with sinusoidal modal shapes.

Focusing on the influence of beam width on beam buckling loads, a relationship between the dimensionless critical loads and the beam length-to-width ratio was also found and a new dimensionless parameter $\alpha L/\chi = \alpha b$ was introduced for accounting to beam slenderness, width and half-space stiffness into a unique parameter. For increasing $\alpha b$, the first three dimensionless critical loads of a beam with pinned ends turned out to converge to the corresponding numerical solutions of a beam on elastic half-plane already obtained by Tullini et al. (2013a), where the third dimensionless critical load is also in agreement with Reissner solution for the buckling of a beam with infinite length (Biot, 1937), which is often adopted for describing the buckling of thin coatings in plane strain conditions and to define the corresponding critical stresses.

Approximated expressions for fitting the numerical results were proposed for the first three dimensionless critical loads of pin-ended beams and for the buckling wavelength of sliding-ended beams, in order to obtain generalized formulas for estimating the minimum critical loads and the critical wavelength of beams on an elastic continuum. In particular, the proposed expression for the buckling wavelength turned out to be more accurate than existing analogous formulas and in agreement with existing laboratory tests.

## ACKNOWLEDGMENTS

The present investigation was developed in the framework of the Research Program FAR 2021 of the University of Ferrara.

## REFERENCES

Allen, H.G., 1969. Analysis and Design of Structural Sandwich Panels. Pergamon Press, Oxford.

Anyaegbunam, A.J., 2014. Complete stress and displacements in a cross-anisotropic half-space caused by a surface vertical point load. Int. J. Geomech. 14(2), 171–181.

Argatov, I., Mishuris, G., 2018. Indentation Testing of Biological Materials. Springer, Cham.

Baraldi, D., 2019. Static and buckling analysis of thin beams on an elastic layer. Comp. Mech. Comput. Appl. Int. J. 10(3), 187–211.

Baraldi, D., Tullini, N., 2017. Incremental analysis of elastoplastic beams and frames resting on an elastic half-plane. J. Eng. Mech. 143(9), 04017101, 1–9.

Baraldi, D., Tullini, N., 2018. In-plane bending of Timoshenko beams in bilateral frictionless contact with an elastic half-space using a coupled FE-BIE method. Eng. Anal. Bound. Elem. 97, 114–130.

Baraldi, D., Tullini, N., 2020. Static stiffness of rigid foundation resting on elastic half-space using a Galerkin boundary element method. Eng. Struct. 225, 111061, 1–14.

Bielak, J., Stephan, E., 1983. A modified Galerkin procedure for bending of beams on elastic foundations. SIAM J. Sci. Stat. Comput. 4(2), 340–352.

Biot, M.A., 1937. Bending of an infinite beam on an elastic foundation. J. Appl. Mech. 4, A1–A7.

Bowden, N., Huck, W.T.S., Paul, K.E., Whitesides, G.M., 1999. The controlled formation of ordered, sinusoidal structures by plasma oxidation of an elastomeric polymer. Appl. Phys. Lett. 75(17), 2557–2559.

Davies, J.M., 2001. Lightweight Sandwich Construction. Blackwell Science, Oxford.

Ding, H., Chen, W., Zhang, L., 2006. Elasticity of Transversely Isotropic Materials. Springer, Dordrecht.

Erwin, V.J., Stephan, E.P., 1992. Adaptive approximations for 3-D electrostatic plate problems. Adv. Eng. Software 15(3–4), 211–215.

Falope, F.O., Lanzoni, L., Radi, E., 2020. Buckling of a Timoshenko beam bonded to an elastic half-plane: Effects of sharp and smooth beam edges Int. J. Solids Struct. 185–186, 222–239.

Genzer, J., Groenewold, J., 2006. Soft matter with hard skin: from skin wrinkles to templating and material characterization. Soft Matter 2, 310–323.

Goodier, J.N., Hsu, C.S., 1954. Nonsinusoidal buckling modes of sandwich plates. J. Aeronaut. Sci. 21, 525–532.

Gough, G.S., Elam C.F., de Bruyne, N.A., 1940. The stabilisation of a thin sheet by a continuous supporting medium. J. R. Aeronaut. Soc. 44, 12–43.

Graham, I.G., McLean, W., 2006. Anisotropic mesh refinement: the conditioning of Galerkin boundary element matrices and simple preconditioners. SIAM J. Numer. Anal. 44(4), 1487–1513.

Gurtin, M.E., Sternberg, E., 1961. Theorems in linear elastostatics for exterior domains. Arch. Ration. Mech. Anal. 8, 99–119.

Hetenyi, M., 1946. Beam on Elastic Foundation. University of Michigan Press, Michigan.

Huang, R., 2005, Kinetic wrinkling of an elastic film on a viscoelastic substrate. J. Mech. Phys. Solids 53(1), 63–89.

Huang, R., Suo, Z., 2002a. Instability of a compressed elastic film on a viscous layer. Int. J. Solids Struct. 39(7), 1791–1802.

Huang, R., Suo, Z., 2002b. Wrinkling of a compressed elastic film on a viscous layer. J. Appl. Phys. 91(3), 1135–1142.

Jiang, H., Khang, D.Y., Fei, H., Kim, H., Huang, Y., Xiao, J., Rogers, J.A., 2008. Finite width effect of thin-films buckling on compliant substrate: Experimental and theoretical studies. J. Mech. Phys. Solids 56, 2585–2598.

Johnson, K.L., 1985. Contact mechanics. Cambridge University Press, Cambridge.

Kachanov, M.L., Shafiro, B., Tsukrov, I., 2003. Handbook of elasticity solutions. Kluwer Academic Publishers, Dordrecht.

Kerr, A.D., 1974. The stress and stability analyses of railroad tracks. ASME J. Appl. Mech. 41, 841–848.

Kerr, A.D., 1978. Analysis of thermal track buckling in the lateral plane. Acta Mech. 30, 17–50.

Kerr, A.D., 1984. Shade, P.J., Analysis of concrete pavement blowups. Acta Mech. 52, 201–224.

Kikuchi, N., 1980. Beam bending problems on a Pasternak foundation using reciprocal variational-inequalities. Q. Appl. Math. 38(1), 91–108.

Kikuchi, N., Oden, J., 1988. Contact problems in elasticity. A study of variational inequalities and finite element methods. SIAM, Philadelphia.

Ley, R.P., Lin W., Mbanefo, U., 1999. Facesheet wrinkling in sandwich structures, NASA, CR-1999-208994, Virginia.

Liao, J.H., Wang, C., 1998. Elastic solutions for a transversely isotropic half-space subjected to a point load. Int. J. Numer. Anal. Meth. Geomech. 22, 425–447.

Lim, N.-H., Park, N.-H., Kang, Y.-J., 2003. Stability of continuous welded rail track. Comp. Struct. 81, 2219–2236.

Marmo, F., Toraldo, F., Rosati, L., 2017. Transversely isotropic half-spaces subject to surface pressures. Int. J. Solids Struct. 104–105, 35–49.

Michell, J.H., 1900. The stress in an æolotropic elastic solid with an infinite plane boundary. Proc. Lond. Math. Soc. 32, 247–258.

Murthy, G.K.N., 1973. Buckling of continuously supported beams. J. Appl. Mech. 40(2), 546–552.

Popov, V.L., Heß, M., Willert, E., 2019. Handbook of Contact Mechanics. Exact Solutions of Axisymmetric Problems. Springer, Berlin.

Prager, W., 1927. Zur Theorie elastische gelagerter Konstruktionen. Z. Angew. Math. Mech. 7(5), 354–360.

Reddy, J.N., 2006. An Introduction to the Finite Element Method, 3rd Ed. McGraw Hill, Singapore.

Reissner, M.E., 1937. On the theory of beams resting on a yielding foundation. P. N. A. S. 23(6), 328–333.

Selvadurai, A.P.S., 1979a. Elastic analysis of soil-foundation interaction. Elsevier, Developments in Geotechnical Engineering, Amsterdam.

Selvadurai, A.P.S., 1979b. The interaction between a uniformly loaded circular plate and an isotropic elastic halfspace: a variational approach. J. Struct. Mech. 7(3), 231–246.

Selvadurai, A.P.S., 1980. Elastic contact between a flexible circular plate and a transversely isotropic elastic halfspace. Int. J. Solids Struct. 16, 167–176.

Selvadurai, A.P.S., 1984. A contact problem for a Reissner plate and an isotropic elastic halfspace. J. Mech. Theor. Appl. 3(2), 181–196.

Shield, T.W., Kim, K.S., Shield, R.T., 1994. The buckling of an elastic layer bonded to an elastic substrate in plane strain. ASME J. Appl. Mech. 61, 231–235.

Stafford, C.M., Harrison, C. , Beers, K.I., Karim, A., Amis, E.J., Vanlandingham, M.R., Kim, H.C., Volksen, W., Miller, R.D., Simonyi, E.E., 2004. A buckling-based metrology for measuring the elastic moduli of polymeric thin films. Nat. Mater. 3(8), 545–550.

Tarasovs, S. Andersons, J., 2008. Buckling of a coating strip of finite width bonded to elastic half-space. Int. J. Solids Struct. 45(2), 593–600.

Timoshenko, S.P., Gere, J.M., 1961. Theory of Elastic Stability. McGraw-Hill, New York.

Tezzon, E., Tralli, A., Tullini, N., 2018. Debonding of FRP and thin films from an elastic half-plane using a coupled FE-BIE model. Eng. Anal. Bound. Elem. 93, 21–28.

Tezzon, E., Tullini, N., Lanzoni, L., 2016. A coupled FE-BIE model for the static analysis of Timoshenko beams bonded to an orthotropic elastic half-plane. Eng. Anal. Bound. Elem. 71, 112–128.

Tezzon, E., Tullini, N., Minghini, F., 2015. Static analysis of shear flexible beams and frames in adhesive contact with an isotropic elastic half-plane using a coupled FE-BIE model. Eng. Struct. 104, 32–50.

Tullini, N., Tralli, A., 2010. Static analysis of Timoshenko beam resting on elastic half-plane based on the coupling of locking-free finite elements and boundary integral. Comput. Mech. 45(2–3), 211–225.

Tullini, N., Tralli, A., Baraldi, D., 2013a. Stability of slender beams and frames resting on 2D elastic half-space. Arch. Appl. Mech. 83(3), 467–482.

Tullini, N. Tralli, A., Baraldi, D., 2013b. Buckling of Timoshenko beams in frictionless contact with an elastic half-plane. J. Eng. Mech. 139(7), 824–831.

Tullini, N. Tralli, A., Lanzoni, L., 2012. Interfacial shear stress analysis of bar and thin film bonded to 2D elastic substrate using a coupled FE-BIE method. Finite Elem. Anal. Des. 55, 42–51.

Vesic, A.B., 1961. Bending of beams on isotropic elastic medium. J. Eng. Mech. 87(EM2), 35–53.

Volynskii, A.L., Bazhenov, S., Lebedeva, O.V., Bakeev, N.F., 2000. Mechanical buckling instability of thin coatings deposited on soft polymer substrates. J. Mater. Sci. 35, 547–554.

Wang, C., Zhang, S., Nie, S., Su, Y., Chen, W., Song, J., 2020. Buckling of a stiff thin film on a bi-layer compliant substrate of finite thickness. Int. J. Solids Struct. 188–189, 133–140.

Wieghardt, K., 1922. Über den Balken auf nachgiebiger Unterlage. Z. Angew. Math. Mech. 2(3), 165–184.

Wilder, E.A., Guo, S., Lin-Gibson, S., Fasolka, M.J., Stafford, C.M., 2006. Measuring the modulus of soft polymer networks via a buckling-based metrology. Macromolecules 39(12), 4138–4143.

Winkler, E., 1867. Die Lehre von der Elastizität und Festigkeit. Dominicus, Prague.

**Figure captions**

Fig. 1. Compressed beam resting on semi-infinite three-dimensional half-space.

Fig. 2. Relative differences for the first three critical loads versus the overall number subdivisions along beam length for a compressed beam with free ends with $\alpha L$ = 5 (a, c) and 25 (b, d), with $\chi = 10$

Fig. 3. Dimensionless critical loads $P_{\mathrm{cr},s}$ versus $\alpha L$ for a beam with sliding ends on elastic half-space.

Fig. 4. First (continuous line) and second (dashed line) mode shapes for a beam with sliding ends and $\alpha L$ equal to 5 (a) and 25 (b).

Fig. 5. Dimensionless critical loads $P_{\mathrm{cr},p}$ versus $\alpha L$ for a beam with pinned ends on elastic half-space.

Fig. 6. First (continuous line) and second (dashed line) mode shapes for a beam with pinned ends on half-space and $\alpha L$ equal to 5 (a), 10 (b), 25 (c) and 50 (d).

Fig. 7. Dimensionless critical loads $P_{\mathrm{cr},f}$ versus $\alpha L$ for a beam with free ends on elastic half-space.

Fig. 8. First (continuous line) and second (dashed line) mode shapes for a beam with free ends and $\alpha L$ equal to 1 (a), 5 (b), 10 (c) and 25 (d).

Fig. 9. First three dimensionless critical loads of a beam on half-space versus $\alpha L/\chi$.

Fig. 10. Second mode shape for a beam with pinned ends, $\alpha L = 50$ and increasing $\chi$.

Fig. 11. Determination of buckling wavelength corresponding to the minimum critical load for $-L/4 \leq x \leq L/4$, for two $\alpha L$ and $\chi$ cases.

Fig. 12. Buckling wavelength of beams with sliding ends on elastic half-space versus $\alpha L$ and varying $\chi$ (a); with respect to the wavelength of a beam on elastic half-plane versus $\alpha L/\chi$ (b).

Fig. 13. Buckling wavelength corresponding to $P_{\mathrm{cr},p,2}$ with respect to the wavelength of a beam on elastic half-plane versus $\alpha L/\chi$.

**Table captions**

Tab. 1. Reference critical loads for a compressed beam with free ends on elastic half-space, obtained with $n_x = 2^{11}$ and a power-graded subdivision along y direction with $n_y = 7$ and $\beta = 3$.

Tab. 2. Dimensionless critical loads of a beam on half-space with $\alpha L = 50$ varying $\chi$.